The difference in immunohistochemical reactivity of monoclonal antibodies against amino-terminal residues of amyloid-β peptide

Short title: Differential immunohistochemical reactivity of anti-Aβ antibodies

Kana Araki[1, 2], Kenta Yamauchi[1, 2*], Shogo Ito[1, 2], Masato Koike[1] and Hioki Hiroyuki[1, 2, 3*]

[1]Department of Neuroanatomy, Juntendo University Graduate School of Medicine, Bunkyo-Ku, Tokyo, Japan

[2]Department of Cell Biology and Neuroscience, Juntendo University Graduate School of Medicine, Bunkyo-Ku, Tokyo, Japan

[3]Department of Multi-Scale Brain Structure Imaging, Juntendo University Graduate School of Medicine, Bunkyo-Ku, Tokyo, Japan

*Corresponding Authors

E-mail: ke-yamauchi@juntendo.ac.jp (KY) and h-hioki@juntendo.ac.jp (HH)

Author contributions

Conceptualization, K.A., K.Y. and S.I.; Methodology, K.A., K.Y. and S.I.; Investigation, K.A., K.Y., S.I. and H.H.; Formal Analysis, K.A., K.Y. and S.I.; Writing – Original Draft, K.Y.; Writing – Review & Editing, K.A., K.Y., S.I., M.K. and H.H.; Visualization, K.A., and K.Y.; Project Administration, K.Y.; Funding Acquisition, K.Y., S.I., M.K. and H.H..

Abstract

Immunohistochemistry for amyloid-β (Aβ) peptide is an indispensable method for Alzheimer's disease (AD) research. Despite a wide variety of available antibodies against the peptides, the difference of immunohistochemical reactivity is not fully described among anti-Aβ antibodies. Immunohistochemical reactivity of Abs against Aβ peptides is critical for accurate and reliable evaluation of Aβ burden in patients as well as models of AD. Here, we examined immunohistochemical reactivity of two mouse and one rabbit monoclonal antibodies against Aβ N-terminal regions using two AD mouse models, $App^{NL\text{-}F}$ and $App^{NL\text{-}G\text{-}F}$. 6E10, 82E1 and D54D2 Aβ antibodies were used in this study. We found significant differences in the immunohistochemical reactivity in both $App^{NL\text{-}F}$ and $App^{NL\text{-}G\text{-}F}$ models. While 6E10 immunoreactivity was mainly localized to Aβ plaques, D54D2 and 82E1 antibodies stained much more broadly beyond plaques. Interestingly, the latter two Abs showed blurred filamentous immunoreactivity beyond amyloid plaque cores. Double immunostaining using a tyramide signal amplification method, Fluorochromized Tyramide-Glucose Oxidase (FT-GO), suggested that the differential immunohistochemical outcomes were only partially attributable to their sensitivity. Moreover, heat induced epitope retrieval (HIER) did not affect the differential immunohistochemical outcomes. Our analysis indicates that outcomes of Aβ immunohistochemistry highly depends on the antibody used in the study.

Introduction

A major histopathological hallmark of Alzheimer's disease (AD) is deposition of amyloid-β (Aβ) peptides in the brain (1). Aβ peptide is produced through proteolytic processing of a transmembrane protein, amyloid precursor protein (APP) (2, 3). While β-secretase cuts on the N-terminal end of the Aβ peptide, γ-secretase cleaves APP protein at multiple sites at the C-terminal ends to give rise to heterogeneous Aβ species. Aβ peptide is highly fibrillogenic and aggregates into higher-order species such as oligomers, protofibrils, fibrils and plaques, which have detrimental effects on brain integrity (2, 3). More than 30 mutations in APP gene have been reported to cause familial Alzheimer's disease (FAD) (4). Aβ pathology precedes the clinical onset of dementia by over 20 years (5). These findings support the amyloid cascade hypothesis positing that deposition of Aβ plaques in the brain triggers a cascade of events that leads to neurodegeneration (6, 7). The recent successes of Aβ-immunotherapy trials further strengthen the hypothesis (8).

Among multiple Aβ imaging techniques, immunohistochemistry (IHC) with antibodies (Abs) against Aβ peptides is superior in sensitivity and specificity (9) and widely used for measuring Aβ load in AD patients as well as models. Microscopic examination of IHC staining for Aβ peptides is further utilized for the definitive diagnosis and neuropathological staging of AD in postmortem brains (9, 10). Various kinds of Abs against Aβ peptides have been developed over the past decades and adapted for IHC analysis (11-16). They show differences in clonality, host species, target amino acid sequences and modification. However, there is no consensus on which Abs should be used for the detection of Aβ peptide by IHC. Critically, the difference in IHC reactivity among anti-Aβ Abs are not fully described. The differential IHC reactivity of the Abs should affect neuropathologic analysis of Aβ deposition by IHC staining.

Here, we examined IHC reactivity of two mouse monoclonal and one rabbit monoclonal Abs against N-terminal residues of human Aβ peptides using two *App* knock-in (KI) mouse models. These Abs showed significant differences in both mouse models regarding IHC outcomes. We further asked

66 whether the differences could be attributable to their sensitivity and antigen masking.

Materials and Methods

Animals

This study was carried out in strict accordance with Fundamental Guidelines for Proper Conduct of Animal Experiments by the Science Council of Japan (2006). All animal procedures were conducted in compliance with ARRIVE (Animal Research: Reporting *In Vivo* Experiments) guidelines. The protocol was approved by the Institutional Animal Care and Use Committees of Juntendo University (Approval No. 2023194). All surgery was performed under sodium pentobarbital anesthesia, and all efforts were made to minimize suffering.

Male $App^{NL\text{-}G\text{-}F/NL\text{-}G\text{-}F}$ (17) mice (RBRC06344, RIKEN BioResource Research Center) at 14 months old were used. The mice were housed in 12/12 h light/dark cycle at 20–25 °C under specific pathogen-free conditions and given access to food and water ad libitum. Mice were euthanized immediately if they reached the humane endpoints: self-mutilation, breathing problems/cyanosis or inability to access food or water. Animal health and behavior were monitored twice a week. Three randomly selected mice were subjected to immunohistochemical examination. The duration of the experiments was set to 14 months. All mice survived during the duration of the experiments.

Tissue preparation

Anesthesia was induced by intraperitoneal injection of an overdose of sodium pentobarbital (200 mg/kg; P0776, Tokyo Chemical Industry) in accordance with American Veterinary Medical Association (AVMA) Guidelines for the Euthanasia of Animals (2020). Following assessment of adequate depth of anesthesia by eye-blink reflexes and toe-pinch withdrawal, the thorax was opened and the right atrium was cut to allow drainage. The heart was perfused with 20 mL of ice-cold phosphate-buffered saline (PBS), followed by 20 mL of ice-cold 4% paraformaldehyde (1.04005.1000, Merck Millipore) in 0.1 M phosphate buffer (PB; pH 7.4). Brains were removed from the skull,

91 postfixed in the same fixative overnight and cryoprotected in 30% sucrose in 0.1 M PB at 4 °C. Fixed
92 brains of male *App*$^{NL\text{-}F/NL\text{-}F}$ (17) mice (RBRC06343, RIKEN BioResource Research Center) at 14
93 months old were provided by Dr. A. Miyawaki (RIKEN Center for Brain Science). The brains were
94 mounted on a freezing microtome (REM-710; Yamato Kohki Industrial) and cut into 30-μm-thick
95 coronal sections (18).
96

97 # IHC staining

98 IHC was performed by a free-floating method at 20–25 °C (19). The primary and secondary
99 Abs used are listed in S1 and S2 Tables respectively. Abs and streptavidin were diluted in 0.3% Triton
100 X-100 in PBS (PBS-X) containing 0.12% λ-carrageenan (035-09693; Sigma-Aldrich) and 1% normal
101 donkey serum (S30-100ML, Merck Millipore). Heat induced epitope retrieval (HIER) was
102 accomplished by overnight incubation at 60 °C in a citrate buffer (ab93678, abcam) prior to IHC
103 staining. Brain sections immunostained for Aβ were mounted onto glass slides (Superfrost micro slide
104 glass APS-coated, Matsunami Glass) and coverslipped with Fluoromount/Plus™ (K048, Diagnostic
105 Biosystems).
106 For single IHC staining with anti-Aβ Abs, brain sections were washed twice for 10 min in
107 PBS-X and reacted overnight with primary Abs. The sections were washed twice for 10 min in PBS-
108 X and reacted for 2 h with secondary Abs. After washing twice for 10 min in PBS-X, the sections were
109 incubated with PBS-X containing FSB (10 or 20 μg/mL, F308, Dojindo) and NeuroTrace 530/615 Red
110 Fluorescent Nissl Stain (1:100, N21482, Thermo Fisher Scientific), and washed twice for 10 min in
111 PBS-X.
112 For double IHC staining with 6E10 and 82E1 or D54D2 Aβ Abs, brain sections were reacted
113 first with 6E10 Ab, and then with biotinylated 82E1 or D54D2 Abs. In double IHC with 6E10 and
114 82E1 mouse monoclonal Abs, Alexa Fluor (AF) 488-conjugated Fab fragments of goat ant-mouse
115 IgG1 Ab (8.0 μg/mL) was applied prior to incubation with the biotinylated 82E1 Ab. AF 568-

116 conjugated streptavidin (2 μg/mL, S11226, Thermo Fisher Scientific) was used for the detection of the
117 biotinylated anti-Aβ Ab. In double IHC with 6E10 and D54D2 Aβ Abs, secondary Abs were
118 simultaneously applied following incubation with D54D2 Ab. After IHC staining, brain sections were
119 stained with FSB as above.

120 Fluorochromized Tyramide-Glucose Oxidase (FT-GO) immunofluorescence (IF) was
121 adapted for sensitive detection of 6E10 Aβ Ab (19). Following incubation for 30 min in PBS
122 containing 1% hydrogen peroxide, brain sections were washed twice for 10 min in PBS-X and reacted
123 overnight with biotinylated 6E10 Ab. The sections were washed twice for 10 min PBS-X, incubated
124 for 2 h in avidin-biotin complex solution (1:500, PK-6100, Vectastain Elite ABC kit, Vector
125 Laboratories), and washed twice for 10 min in PBS-X and twice for 5 min in 0.1 M PB. Then, the
126 sections were incubated for 10 min with an FT-GO reaction mixture which contained 10 μM CF568
127 tyramide (92173, Biotium). FT-GO reaction was initiated by adding β-D-glucose (16804-32, Nacalai
128 Tesque) into the mixture at 2 mg/mL and proceeded for 30 min. Following two washes in PBS-X for
129 10 min each, the sections were reacted overnight with a complex of 82E1 Ab (1.0 μg/mL) and AF 488-
130 conjugated Fab fragments of goat ant-mouse IgG1 Ab (1.0 μg/mL) and washed twice for 10 min in
131 PBS-X. The primary and secondary Ab complex was prepared following the manufacturer instruction.
132 In the indirect detection compared with FT-GO signal amplification, unconjugated 6E10 Ab and
133 Rhodamine Red X-conjugated Fab fragments of goat ant-mouse IgG1 Ab were used as primary and
134 secondary Abs, respectively. Brain sections were reacted with these Abs prior to incubation with 82E1
135 Ab.

136

137 Image acquisition and processing

138 Images were captured with a confocal laser scanning microscope (TCS SP8; Leica
139 Microsystem). A 16× multi-immersion (HC FLUOTAR 16x/0.60 IMM CORR VISIR, NA = 0.60,
140 Leica Microsystems) and 25× water-immersion (HC FLUOTAR L 25x/0.95 W VISIR, NA = 0.95,

141 Leica Microsystems) objective lenses were used. The confocal pinhole was adjusted to 1.0 or 2.0 Airy
142 unit. Z-stack images were collected at 1.5 to 8.0 μm intervals at 512×512 or 1,024×1,024 pixel
143 resolutions. Captured images were stitched and processed to create maximum intensity projection
144 images using Leica Application Suite X software (LAS X, ver. 3.5.5.19976, Leica Microsystems). The
145 brightness and contrast of images were adjusted using Fiji software (20) (ver. 2.14.0/1.54 f).
146

147 # Quantification

148 To assess IHC reactivity of 6E10, 82E1 and D54D2 Aβ Abs, immunohistochemically stained
149 area (IHCSA) of each Ab was measured in the cerebral cortex and hippocampus using Fiji software.
150 After subtracting background noise, the number of pixels above a threshold was counted and
151 designated as the IHCSA. The threshold was set manually for each image. The IHCSA was normalized
152 to the FSB-stained area, a proxy for Aβ load in each brain section. In the cerebral cortex, the IHCSA
153 was analyzed in the region which is located medial to the outer edge of CA3 pyramidal cell layer and
154 lateral to the inner edge of the dentate gyrus (DG) granule cell layer. The hippocampus was analyzed
155 in its entirety. For direct comparisons of staining properties between 6E10 and 82E1 or D54D2 Aβ
156 Abs, FSB-labeled plaques were randomly selected from the cerebral cortex of $App^{NL\text{-}F/NL\text{-}F}$ mice.
157 To assess effects of signal amplification resulting from FT-GO IF and antigen unmasking
158 with HIER, IHCSA of 6E10 or 82E1 Aβ Abs was measured and quantified in the cerebral cortex of
159 $App^{NL\text{-}F/NL\text{-}F}$ mice as above. The coverage area of 82E1 IHCSA by 6E10 IHCSA was calculated using
160 Fiji software. The region medial to the outer edge of CA3 pyramidal cell layer and lateral to the inner
161 edge of the DG granule cell layer was subjected to analysis.
162

163 # Statistical analysis

164 Statistical analyses were conducted using GraphPad Prism 9 software (Version 9.4.1 (458),
165 GraphPad Software). For comparisons among independent groups, Brown-Forsythe and Welch one-

166 way analysis of variance (ANOVA) followed by Tukey-Kramer post hoc test (*App*$^{NL\text{-}G\text{-}F/NL\text{-}G\text{-}F}$ mouse
167 hippocampus) or Kruskal-Wallis test followed by Dunn's post hoc test (*App*$^{NL\text{-}F/NL\text{-}F}$ mouse cerebral
168 cortex and hippocampus, and *App*$^{NL\text{-}G\text{-}F/NL\text{-}G\text{-}F}$ mouse cerebral cortex) were used. Wilcoxon test was
169 used for paired comparisons between groups (Direct comparisons between 6E10 and 82E1 or D54D2
170 Abs). For comparisons between two independent groups with a normal distribution, unpaired t test was
171 used (FT-GO signal amplification and antigen unmasking using HIER). All tests were two-sided.
172 Statistical significance was set at $P < 0.05$. Graphed data are represented as means ± standard
173 deviations (SDs).

174 IHCSA of 6E10, 82E1 and D54D2 Aβ Abs were examined in seven to nine sections from
175 three *App*$^{NL\text{-}F/NL\text{-}F}$ and *App*$^{NL\text{-}G\text{-}F/NL\text{-}G\text{-}F}$ mice. Thirty plaques in nine brain sections from three *App*$^{NL\text{-}}$
176 $^{F/NL\text{-}F}$ mice were used for direct comparisons between 6E10 and 82E1 or D54D2 Aβ Abs. Nine sections
177 from three *App*$^{NL\text{-}F/NL\text{-}F}$ mice were used to evaluate signal enhancement in 6E10 FT-GO IF and antigen
178 unmasking using HIER. The exact values of n are stated in the corresponding figure legends. Unusual
179 outliers were not found in the datasets.

180

181 # Data availability

182 The datasets generated during and/or analyzed during the current study and all biological
183 materials reported in this article are available from the corresponding authors on reasonable request.

Results

Differential IHC reactivity of N-terminal Aβ Abs

We examined IHC reactivity of monoclonal Abs (mAbs) against N-terminal regions of human Aβ peptide, because 1) N-terminal Aβ Abs are assumed to detect total Aβ peptide in the specimen, 2) diversity of Aβ species generated by γ-secretase cleavage affects IHC outcomes using anti-Aβ Abs against the C-terminal residues (13) and 3) FAD mutations located at the middle of the Aβ sequence can alter binding properties of anti-Aβ Abs that react the region(17). The Aβ Abs studied were 6E10 (21), 82E1 (22) and D54D2 Aβ monoclonal Abs, which all were generated by immunization with N-terminal residues of Aβ peptide and commercially available. Table 1 summarizes host animals, isotypes, immunogens, epitopes and suppliers of these anti-Aβ Abs.

Table 1. Aβ Ab information used in this study

Clone name	Host/Isotype	Immunogen	Epitope	Manufacturer, Cat. No.	RRID
6E10(21)	Mouse/IgG1	Human Aβ 1-16 peptide	Aβ 3–8 peptide	BioLegend, 80301	AB_2565328
82E1(22)	Mouse/IgG1	Human Aβ 1-16 peptide	N-terminus end (Aβ 1–5 peptide)(22)	Immuno-Biological Laboratories, 10323	AB_1630806
D54D2	Rabbit/IgG	Near N-terminus of human Aβ peptide	Not determined	Cell Signaling Technology, 8243S	AB_2797642

We first compared IHC reactivity of these three Abs in *App*$^{NL\text{-}G\text{-}F}$ mouse model (17) (Fig. 1a). Aβ IHC using 6E10, 82E1 and D54D2 Aβ Abs was carried out in frozen brain sections of *App*$^{NL\text{-}G\text{-}F/NL\text{-}G\text{-}F}$ mice. These brain sections were further stained with a Congo-red derivative, 1-Fluoro-2,5-bis(3-carboxy-4-hydroxystyryl)benzene (FSB) (23), to assess Aβ deposition in each brain section. IHC reactivity for Aβ peptides was quite different among 6E10, 82E1 and D54D2 Abs (Fig. 1a). While moderate and scattered immunoreactivity was found in brain sections stained with 6E10 Ab (Fig. 1a$_1$),

203 82E1 and D54D2 Abs labeled more massively and intensely brain sections of *App*$^{NL\text{-}G\text{-}F/NL\text{-}G\text{-}F}$ mice
204 (Fig. 1a$_{2,\,3}$). IHC reactivity were similar between 82E1 and D54D2 Aβ Abs. The same tendency was
205 found in *App*$^{NL\text{-}F/NL\text{-}F}$ mouse models (Fig. 1b), where Aβ burden is much less severe than *App*$^{NL\text{-}G\text{-}F/NL\text{-}}$
206 $^{G\text{-}F}$ mice (17). IHCSA normalized to Aβ fibril deposition assessed by FSB labeling was measured and
207 quantified in the cerebral cortex and hippocampus of both models (Fig. 1c, d). IHCSA of 82E1 and
208 D54D2 Aβ Abs was 2.49 to 4.49 times broader than that of 6E10 Aβ Ab. There were no significant
209 differences in IHCSA between 82E1 and D54D2 Abs (Fig. 1c, d). Additionally, the significant
210 difference in IHCSA was not detected between 6E10 and 82E1 Abs in the hippocampus of *App*$^{NL\text{-}F/NL\text{-}}$
211 ^{F} mice.
212
213 **Fig 1. Differential IHC reactivity among 6E10, 82E1 and D54D2 Aβ Abs.**
214 **a, b**) Aβ IHC in *App*$^{NL\text{-}G\text{-}F/NL\text{-}G\text{-}F}$ (**a**) and *App*$^{NL\text{-}F/NL\text{-}F}$ (**b**) mouse brain sections. 6E10 (**a$_1$, b$_1$**), 82E1 (**a$_2$,**
215 **b$_2$**) and D54D2 (**a$_3$, b$_3$**) Aβ Abs are used for the IHC. **c, d**) Histograms showing The IHCSA of 6E10,
216 82E1 and D54D2 Abs in *App*$^{NL\text{-}G\text{-}F/NL\text{-}G\text{-}F}$ (**c**) and *App*$^{NL\text{-}F/NL\text{-}F}$ (**d**) mice. The IHCSA in the cerebral
217 cortex (left) and hippocampus (right) are represented (*App*$^{NL\text{-}G\text{-}F/NL\text{-}G\text{-}F}$: n = 7 sections, 6E10 Ab in the
218 Ctx; n = 7 sections, 82E1 Ab in the Ctx; n = 9 sections, D54D2 Ab in the Ctx from 3 animals; H =
219 14.59, df = 2, P = 0.0009, Kruskal-Wallis test; n = 8 sections, 6E10 Ab in the Hipp; n = 9 sections,
220 82E1 Ab in the Hipp; n = 9 sections, D54D2 Ab in the Hipp from 3 animals; F = 35.42, df = 2, P <
221 0.0001, Brown-Forsythe ANOVA test. *App*$^{NL\text{-}F/NL\text{-}F}$: n = 8 sections, 6E10 Ab in the Ctx; n = 8 sections,
222 82E1 Ab in the Ctx; n = 9 sections, D54D2 Ab in the Ctx from 3 animals; H = 11.88, df = 2, P =
223 0.0026, Kruskal-Wallis test; n = 9 sections, 6E10 Ab in the Hipp; n = 9 sections, 82E1 Ab in the Hipp;
224 n = 9 sections, D54D2 Ab in the Hipp from 3 animals; H = 13.91, df = 2, P = 0.001, Kruskal-Wallis
225 test). Data are represented as means ± SDs. Ctx: cerebral cortex, Hipp: hippocampus, Thl: Thalamus.
226 Scale bar: 1000 μm. *P < 0.05; **P < 0.01; ***P < 0.001; ****P < 0.0001.
227

228 We then directly compared IHC reactivity of the anti-Aβ Abs by double IHC staining (Fig.
229 2). We analyzed IHC reactivity in the cerebral cortex of *App*$^{NL\text{-}F/NL\text{-}F}$ mice, because massive Aβ plaque
230 burden in *App*$^{NL\text{-}G\text{-}F/NL\text{-}G\text{-}F}$ mice makes it difficult to examine staining properties of these Abs in detail
231 (Fig. 1a). Given that 82E1 and D54D2 Abs showed comparable IHC reactivity (Fig. 1c, d), IHC
232 reactivity was compared between 6E10 and 82E1 or D54D2 N-terminal Aβ Abs. For this, we
233 conducted sequential double IHC staining. Following incubation of 6E10 Ab, 82E1 or D54D2 Ab was
234 applied to brain sections to prevent the latter two Abs from preoccupying the epitope of 6E10 Ab.
235 Again, 82E1 and D54D2 Abs showed much stronger IHC reactivity than 6E10 Ab in the direct
236 comparison (Fig. 2a, b). Of all analyzed plaques, 82E1 and D54D2 Abs stained broader regions than
237 6E10 Ab did (Fig. 2c, d). IHCSA of 82E1 and D54D2 Abs was 2.67 and 4.25 times broader
238 respectively than that of 6E10 Ab (Fig. 2c, d). Whereas 6E10 immunoreactivity was mainly localized
239 to plaque cores, 82E1 and D54D2 Abs stained much broader regions over amyloid cores visualized by
240 FSB labeling (Fig. 2a, b). Interestingly, 82E1 and D54D2 Abs showed blurred filamentous
241 immunoreactivity beyond plaque cores (Fig. 2a, b). 6E10 IHCSA narrower than the FSB-stained area
242 was found in approximately half of analyzed plaques (33 plaques in 60 plaques).
243
244 **Fig 2. Direct comparisons of IHC characteristics between 6E10 and 82E1 or D54D2 Aβ Abs.**
245 **a, b**) Double IHC with 6E10 and 82E1 (**a**) or D54D2 (**b**) Aβ Abs in the cerebral cortex of *App*$^{NL\text{-}F/NL\text{-}}$
246 ^{F} mice. FSB is used for labeling Aβ fibrils. $\mathbf{a_{1\text{-}4}}$, $\mathbf{b_{1\text{-}4}}$) Representative images for 6E10 Ab (yellow, $\mathbf{a_1}$,
247 $\mathbf{b_2}$), 82E1 (magenta, $\mathbf{a_2}$) or D54D2 Ab (magenta, $\mathbf{b_2}$) and FSB (cyan, $\mathbf{a_3}$, $\mathbf{b_3}$) staining. $\mathbf{a_4}$, $\mathbf{b_4}$) Merged
248 images of ($\mathbf{a_1}$), ($\mathbf{a_2}$) and ($\mathbf{a_3}$), and ($\mathbf{b_1}$), ($\mathbf{b_2}$) and ($\mathbf{b_3}$), respectively. **c, d**) Direct comparisons of IHCSA
249 of 6E10 and 82E1 (**c**) or D54D2 Aβ Abs (**d**) (n = 30 plaques from 9 sections of 3 animals for each;
250 6E10 vs 82E1 Abs: $W = 465.0$, $df = 1$, $P < 0.0001$, Wilcoxon matched-pairs signed rank test; 6E10 vs
251 D54D2 Abs: $W = 465.0$, $df = 1$, $P < 0.0001$, Wilcoxon matched-pairs signed rank test). Data are
252 represented as means ± SDs. Scale bar: 30 μm. ****$P < 0.0001$.

253

254 One possible explanation for the differential IHC outcomes among 6E10, 82E1 and D54D2
255 N-terminal Aβ Abs is the difference of IHC sensitivity of these Abs. If differential IHC sensitivity
256 underlies the differential outcomes of IHC, signal amplification techniques that enhances IHC
257 sensitivity should close the gap of IHC reactivity among Abs. We thus conducted FT-GO IF for 6E10
258 Ab and compared IHC reactivity of 82E1 Ab. FT-GO is a fluorescent tyramide signal amplification
259 system (TSA) technique, yielding 10- to 30-fold signal amplification compared with indirect IHC
260 detection (19). Because the epitope of D54D2 Ab has not been described in detail (Table 1), this Ab
261 was excluded from the analysis. Even after signal amplification by FT-GO, IHCSA of 82E1 Ab was
262 still much broader than that of 6E10 Ab (6E10/82E1^{+} IHCSA in 82E1^{+} IHCSA [means ± SDs]: FT-
263 GO, 0.442 ± 0.081) (Fig. 3). FT-GO signal amplification actually enhanced IHC sensitivity of 6E10
264 Ab: IHCSA of FT-GO detection was significantly broader than that of indirect detection (Fig. 3c)
265 (6E10/82E1^{+} IHCSA in 82E1^{+} IHCSA [means ± SDs]: indirect method, 0.318 ± 0.079; FT-GO, 0.442
266 ± 0.081, P = 0.0046, unpaired t test). These results imply that the difference of IHC sensitivity is only
267 partially attributable to the differential IHC outcomes between 6E10 and 82E1 Abs. We further
268 examined antigen masking effects on the differential IHC reactivity. Antigen retrieval techniques such
269 as HIER is frequently used for Aβ IHC staining to unmask epitopes. However, an HIER procedure did
270 not affect differential IHC outcomes between 6E10 and 82E1 Abs (Fig. 4). The gap of IHC reactivity
271 between 6E10 and 82E1 Abs still remained in brain sections treated with HIER (Fig. 4c) (6E10/82E1^{+}
272 IHCSA in 82E1^{+} IHCSA [means ± SDs]: wo/HIER, 0.362 ± 0.087; w/ HIER, 0.407 ± 0.073, P =
273 0.2454, unpaired t test).

274

275 **Fig 3. Signal amplification characteristics of 6E10 Aβ Ab by FT-GO.**

276 **a, b**) Double IHC with 6E10 and 82E1 Aβ Abs in the cerebral cortex of *App*$^{NL\text{-}F/NL\text{-}F}$ mice. 6E10 (**a**)
277 and Biotin-6E10 Ab (**b**) are detected with an indirect method (**a**) and FT-GO signal amplification (**b**),

278 respectively. 82E1 Ab is labeled with an AF 488 conjugated FabuLight antibody prior to incubation
279 with brain sections. **a_{1-3}, b_{1-3}**) Representative images for 6E10 Ab (yellow, **a_1, b_1**) and 82E1 Ab
280 (magenta, **a_2, b_2**) staining. **a_3, b_3**) Merged images of (**a_1**) and (**a_2**), and (**b_1**) and (**b_2**), respectively. **c**)
281 Histograms representing the proportion of 82E1 IHCSA covered by 6E10 IHCSA (n = 9 sections from
282 3 animals for each; t = 3.288, df = 16, P = 0.0046, unpaired t test). Data are represented as means ±
283 SDs. Scale bar: 50 μm.

284

285 **Fig 4. The effect of antigen unmasking on the differential IHC reactivity between 6E10 and 82E1**
286 **Aβ Abs.**

287 **a, b**) Double IHC with 6E10 and 82E1 Aβ Abs in the cerebral cortex of *App*$^{NL-F/NL-F}$ mice. Double Aβ
288 IHC is performed in non-treated (**a**) and HIER-treated (**b**) brain sections. **a_{1-3}, b_{1-3}**) Representative
289 images for 6E10 Ab (yellow, **a_1, b_1**) and 82E1 Ab (magenta, **a_2, b_2**) staining. **a_3, b_3**) Merged images
290 of (**a_1**) and (**a_2**), and (**b_1**) and (**b_2**), respectively. **c**) Histograms representing the proportion of 82E1
291 IHCSA covered by 6E10 IHCSA (n = 9 sections from 3 animals for each; t = 1.206, df = 16, P =
292 0.2454, unpaired t test). Data are represented as means ± SDs. Scale bar: 50 μm.

293 # Discussion

294 In the present study, we analyzed IHC characteristics of two mouse and one rabbit monoclonal
295 Abs against N-terminal regions of Aβ peptide that recognize several isoforms of Aβ peptide and
296 transgenically expressed human APP. We found significant differences of IHC reactivity among these
297 Abs in both $App^{NL\text{-}F}$ and $App^{NL\text{-}G\text{-}F}$ mouse models: while 6E10 immunosignal was mainly localized to
298 plaque cores labeled by FSB, 82E1 and D54D2 Abs stained much more broadly beyond cores. Our
299 results further implied that the differential IHC outcomes between 6E10 and 82E1 Abs was only
300 partially attributable to IHC sensitivity of these Abs by using a fluorescent TSA system, FT-GO.
301 Antigen unmasking with a HIER technique did not affect the difference of IHC reactivity between
302 6E10 and 82E1 Abs.

303 6E10, 82E1 and D54D2 N-terminal Aβ Abs showed significant differences regarding their
304 IHC characteristics, even despite similarities in their prepared immunogens. These Aβ Abs are widely
305 assumed and used to detect total Aβ peptides. IHCSA of 82E1 and D54D2 Abs was much broader than
306 that of 6E10 Ab (Fig. 1). In contrast to immunoreactivity of 6E10 Ab, which was mainly localized to
307 amyloid cores, 82E1 and D54D2 Abs showed blurred filamentous immunosignals beyond plaque cores
308 in addition to immunoreactivity against core region (Fig. 2). The IHC reactivity against filamentous
309 materials around plaque cores can account for the broader IHCSA of 82E1 and D54D2 Abs. The
310 blurred filamentous immunoreactivity might reflect the deposition of protofibrillar and/or fibrillar
311 forms of Aβ peptides onto the brain (2, 3). Our finding that the coverage area of 82E1 IHCSA by 6E10
312 immunosignals was increased by FT-GO signal amplification indicates that differential IHC sensitivity
313 between 6E10 and 82E1 Abs partially explains their differential IHC outcomes (Fig. 3c). However,
314 the differential IHC sensitivity does not account for most of the difference of IHC reactivity between
315 these two Aβ Abs, because a substantial portion of 82E1 IHCSA was still not covered by 6E10
316 immunosignal even after FT-GO signal amplification (Fig. 3b). Our finding that an HIER procedure
317 failed to fill the gap of IHC reactivity between 6E10 and 82E1 Abs argues against the view that antigen

318 masking effects of formaldehyde fixation causes the differential IHC reactivity between the two Aβ
319 Abs (Fig. 4). The slight difference of epitopes within N-terminal regions of Aβ peptide between 6E10
320 and 82E1 Aβ Abs (Table 1) might generate and/or lose affinities for specific forms of the peptides in
321 frozen brain sections. While the epitope of 6E10 Ab lies within amino acids 3-8 of Aβ peptide, 82E1
322 Ab is an N-terminus end specific antibody (22). We cannot rule out the possibility that stronger signal
323 amplification than FT-GO close the gap completely between 6E10 and 82E1 IHCSA.

324 We found differential IHC characteristics of anti-Aβ Abs in both $App^{NL\text{-}G\text{--}F}$ and $App^{NL\text{-}F}$
325 mouse models (Fig. 1). $App^{NL\text{-}G\text{-}F}$ model which harbors Swedish (KM670/671NL), Beyreuther/Iberian
326 (I716F) and Arctic (E693G) mutations is being used most frequently as it develops Aβ pathology much
327 faster than other *App* knock-in lines (24). Aβ sequence of $App^{NL\text{-}F}$ model, which carries the Swedish
328 and Beyreuther/Iberian mutations, is identical to that of wild-type human (17). We consider that our
329 findings of significant differences of IHC characteristics among 6E10, 82E1 and D54D2 Abs could be
330 extrapolatable to other mouse models of AD which express APP FAD mutants transgenically, because
331 the most commonly used mutations in these FAD mutant models are the Swedish and/or
332 Beyreuther/Iberian mutations that are carried by $App^{NL\text{-}G\text{-}F}$ and $App^{NL\text{-}F}$ mouse models (25). Notably,
333 Aβ42 filament structure in $App^{NL\text{-}F}$ model are identical to type II filaments from human brains (26).
334 Further studies are required to determine whether the difference of IHC reactivity among Aβ Abs is
335 also found in the brain of AD patients.

336

337 # Conclusions

338 A wide variety of anti-Aβ Abs developed over the past decades make the knowledge about
339 IHC reactivity of Abs against Aβ peptides important for accurate and reliable evaluation of Aβ plaque
340 burden in patients as well as models of AD. Our results demonstrate that Aβ IHC outcomes highly
341 depend on what kind of Ab is used for the analysis. This could be of importance for meta-analysis

342 where the results of Aβ IHC staining using various kinds of Abs are pooled.

Acknowledgements

We thank Drs. Hiroshi Hama (RIKEN Center for Brain Science) and Atsushi Miyawaki (RIKEN Center for Brain Science) for their kind provision of *App*$^{NL\text{-}F/NL\text{-}F}$ mouse brains; and Drs. Takashi Saito (Nagoya City University) and Takaomi C Saido (RIKEN Center for Brain Science) for sharing *App*$^{NL\text{-}G\text{-}F}$ mice. K.A. is supported by Juntendo Specialized Training for Aspiring Researchers (J-STAR) program at Juntendo University School of Medicine.

References

1. Scheltens P, De Strooper B, Kivipelto M, Holstege H, Chetelat G, Teunissen CE, et al. Alzheimer's disease. Lancet. 2021;397(10284):1577-90.

2. Chen GF, Xu TH, Yan Y, Zhou YR, Jiang Y, Melcher K, et al. Amyloid beta: structure, biology and structure-based therapeutic development. Acta Pharmacol Sin. 2017;38(9):1205-35.

3. Hampel H, Hardy J, Blennow K, Chen C, Perry G, Kim SH, et al. The Amyloid-beta Pathway in Alzheimer's Disease. Mol Psychiatry. 2021;26(10):5481-503.

4. Hunter S, Brayne C. Understanding the roles of mutations in the amyloid precursor protein in Alzheimer disease. Mol Psychiatry. 2018;23(1):81-93.

5. Long JM, Holtzman DM. Alzheimer Disease: An Update on Pathobiology and Treatment Strategies. Cell. 2019;179(2):312-39.

6. Hardy JA, Higgins GA. Alzheimer's disease: the amyloid cascade hypothesis. Science. 1992;256(5054):184-5.

7. Selkoe DJ, Hardy J. The amyloid hypothesis of Alzheimer's disease at 25 years. EMBO Mol Med. 2016;8(6):595-608.

8. Jucker M, Walker LC. Alzheimer's disease: From immunotherapy to immunoprevention. Cell. 2023;186(20):4260-70.

9. DeTure MA, Dickson DW. The neuropathological diagnosis of Alzheimer's disease. Mol Neurodegener. 2019;14(1):32.

368 10. Thal DR, Rub U, Orantes M, Braak H. Phases of A beta-deposition in the human brain and
369 its relevance for the development of AD. Neurology. 2002;58(12):1791-800.
370 11. Masters CL, Multhaup G, Simms G, Pottgiesser J, Martins RN, Beyreuther K. Neuronal origin
371 of a cerebral amyloid: neurofibrillary tangles of Alzheimer's disease contain the same protein as the
372 amyloid of plaque cores and blood vessels. EMBO J. 1985;4(11):2757-63.
373 12. Wong CW, Quaranta V, Glenner GG. Neuritic plaques and cerebrovascular amyloid in
374 Alzheimer disease are antigenically related. Proc Natl Acad Sci U S A. 1985;82(24):8729-32.
375 13. Iwatsubo T, Odaka A, Suzuki N, Mizusawa H, Nukina N, Ihara Y. Visualization of A beta
376 42(43) and A beta 40 in senile plaques with end-specific A beta monoclonals: evidence that an initially
377 deposited species is A beta 42(43). Neuron. 1994;13(1):45-53.
378 14. Murphy GM, Jr., Forno LS, Higgins L, Scardina JM, Eng LF, Cordell B. Development of a
379 monoclonal antibody specific for the COOH-terminal of beta-amyloid 1-42 and its
380 immunohistochemical reactivity in Alzheimer's disease and related disorders. Am J Pathol.
381 1994;144(5):1082-8.
382 15. Yang F, Mak K, Vinters HV, Frautschy SA, Cole GM. Monoclonal antibody to the C-
383 terminus of beta-amyloid. Neuroreport. 1994;5(16):2117-20.
384 16. Saido TC, Iwatsubo T, Mann DM, Shimada H, Ihara Y, Kawashima S. Dominant and
385 differential deposition of distinct beta-amyloid peptide species, A beta N3(pE), in senile plaques.
386 Neuron. 1995;14(2):457-66.

387 17. Saito T, Matsuba Y, Mihira N, Takano J, Nilsson P, Itohara S, et al. Single App knock-in
388 mouse models of Alzheimer's disease. Nat Neurosci. 2014;17(5):661-3.
389 18. Okamoto S, Yamauchi K, Sohn J, Takahashi M, Ishida Y, Furuta T, et al. Exclusive labeling
390 of direct and indirect pathway neurons in the mouse neostriatum by an adeno-associated virus vector
391 with Cre/lox system. STAR Protoc. 2021;2(1):100230.
392 19. Yamauchi K, Okamoto S, Ishida Y, Konno K, Hoshino K, Furuta T, et al. Fluorochromized
393 tyramide-glucose oxidase as a multiplex fluorescent tyramide signal amplification system for
394 histochemical analysis. Sci Rep. 2022;12(1):14807.
395 20. Schneider CA, Rasband WS, Eliceiri KW. NIH Image to ImageJ: 25 years of image analysis.
396 Nat Methods. 2012;9(7):671-5.
397 21. Kim KS, Wen GY, Bancher C, Chen CMJ, Sapienza VJ, Hong H, et al. Detection and
398 Quantitation of Amyloid B-Peptide with 2 Monoclonal-Antibodies. Neuroscience Research
399 Communications. 1990;7(2):113-22.
400 22. Horikoshi Y, Sakaguchi G, Becker AG, Gray AJ, Duff K, Aisen PS, et al. Development of
401 Abeta terminal end-specific antibodies and sensitive ELISA for Abeta variant. Biochem Biophys Res
402 Commun. 2004;319(3):733-7.
403 23. Sato K, Higuchi M, Iwata N, Saido TC, Sasamoto K. Fluoro-substituted and 13C-labeled
404 styrylbenzene derivatives for detecting brain amyloid plaques. Eur J Med Chem. 2004;39(7):573-8.
405 24. Sasaguri H, Hashimoto S, Watamura N, Sato K, Takamura R, Nagata K, et al. Recent

406 Advances in the Modeling of Alzheimer's Disease. Front Neurosci. 2022;16:807473.

407 25. Sasaguri H, Nilsson P, Hashimoto S, Nagata K, Saito T, De Strooper B, et al. APP mouse

408 models for Alzheimer's disease preclinical studies. EMBO J. 2017;36(17):2473-87.

409 26. Yang Y, Arseni D, Zhang W, Huang M, Lovestam S, Schweighauser M, et al. Cryo-EM

410 structures of amyloid-beta 42 filaments from human brains. Science. 2022;375(6577):167-72.

411 # Supporting information

412 **S1 table. Primary Abs used in this study.**

413 **S2 table. Secondary Abs used in this study**

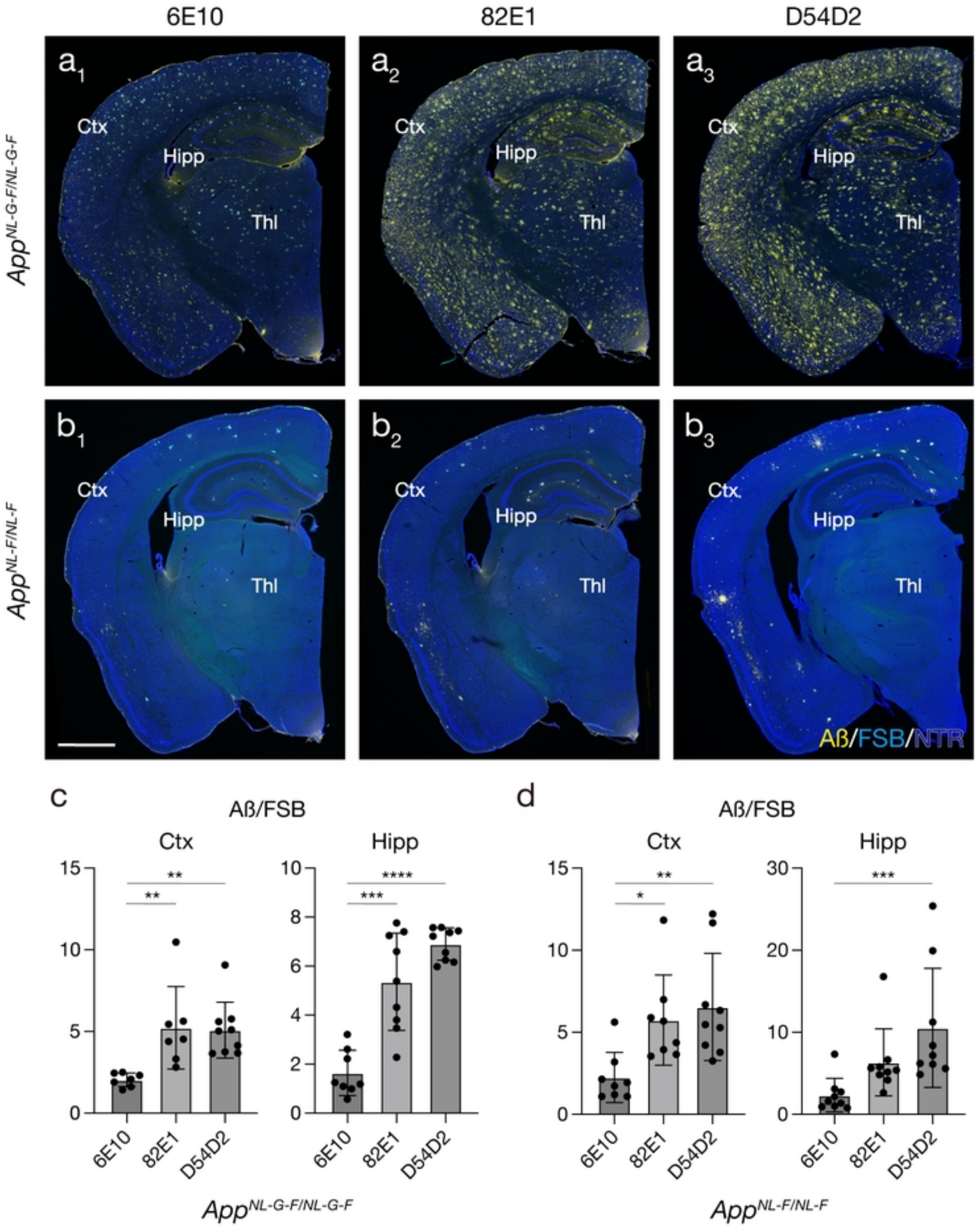
6E10
82E1
D54D2
a1
a2
a3
Ctx
Hipp
Thl
App NL-G-F/NL-G-F
b1
b2
b3
App NL-F/NL-F
Aß/FSB/NTR
c
Aß/FSB
Ctx
Hipp
d
6E10
82E1
D54D2
App NL-G-F/NL-G-F
App NL-F/NL-F

Figure1

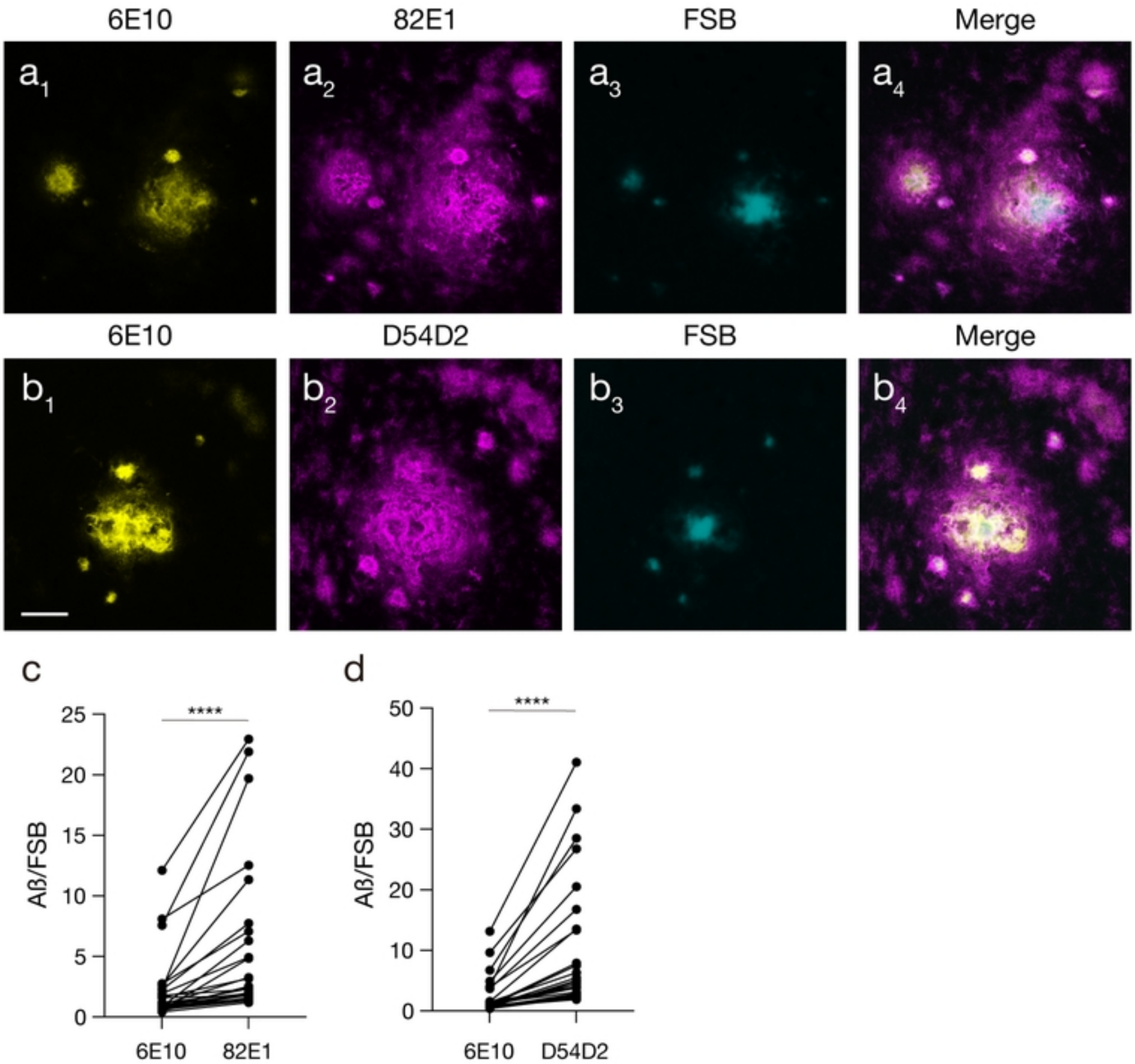
6E10
82E1
FSB
Merge
a1
a2
a3
a4
6E10
D54D2
FSB
Merge
b1
b2
b3
b4
c
d
****
Aß/FSB
25
20
15
10
5
0
6E10
82E1
****
Aß/FSB
50
40
30
20
10
0
6E10
D54D2

Figure2

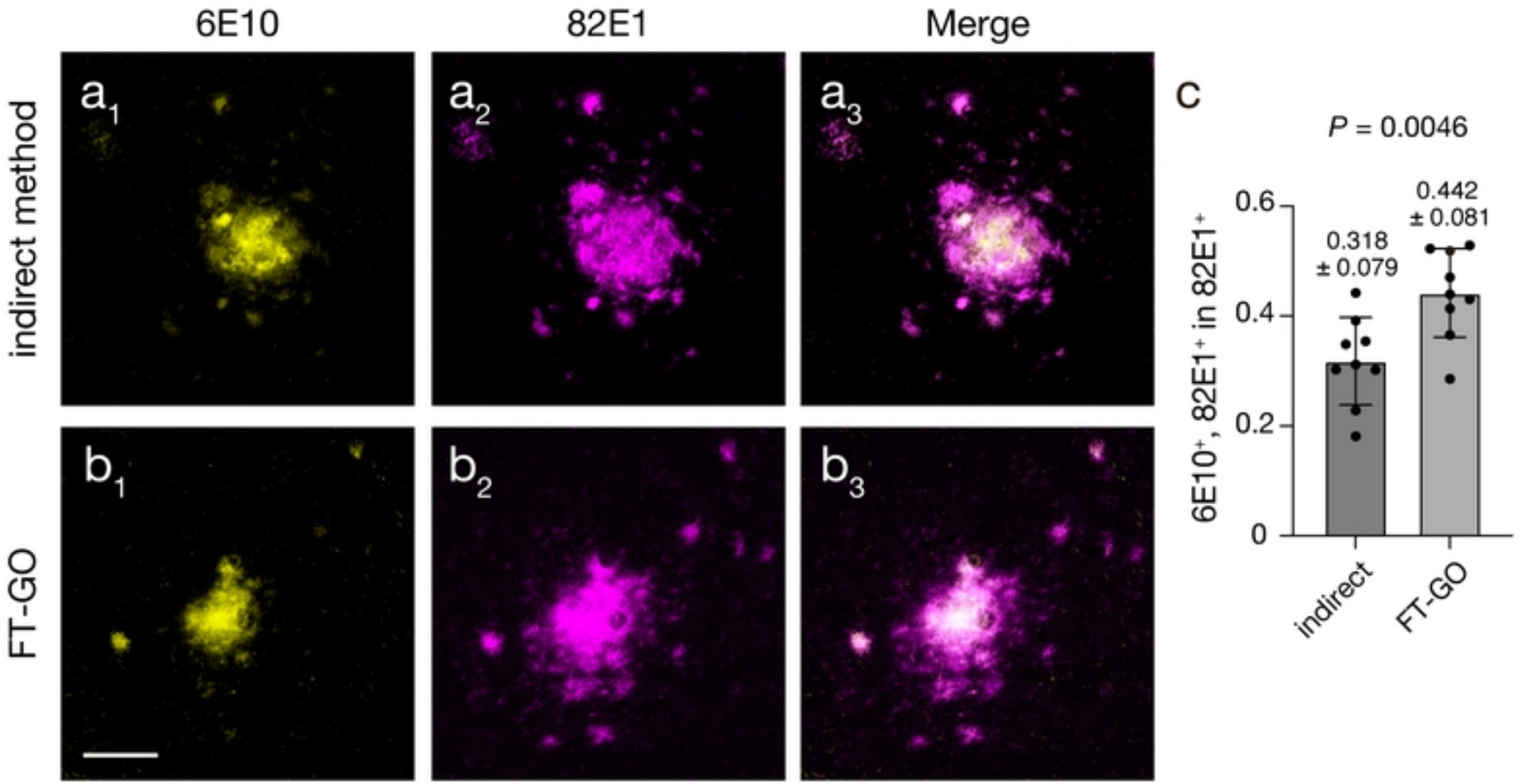
6E10
82E1
Merge
indirect method
FT-GO
a1
a2
a3
b1
b2
b3
c
P = 0.0046
0.318
± 0.079
0.442
± 0.081
6E10+, 82E1+ in 82E1+
0.6
0.4
0.2
0
indirect
FT-GO

Figure3

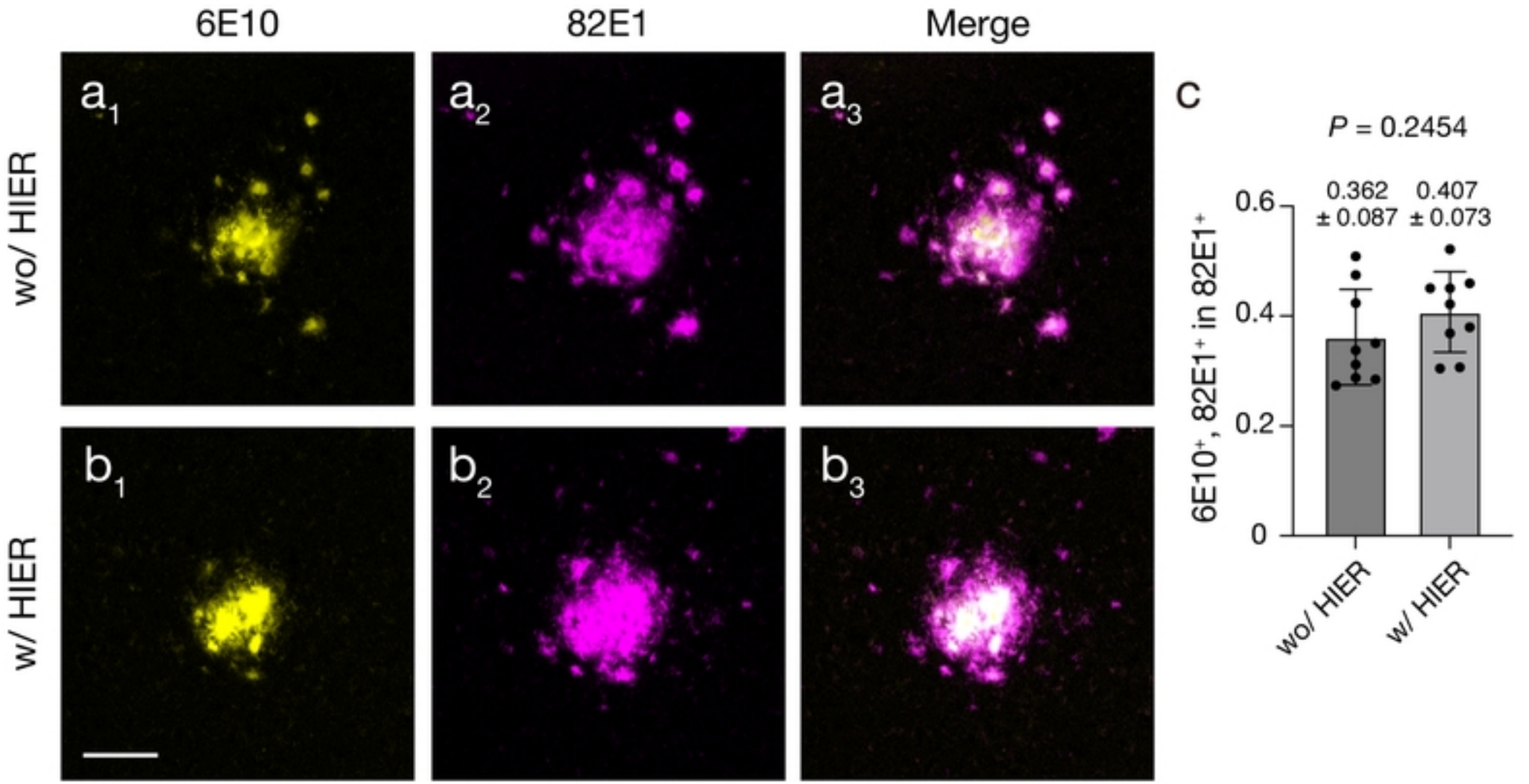
6E10
82E1
Merge
wo/ HIER
w/ HIER
a1
a2
a3
b1
b2
b3
c
P = 0.2454
0.362 ± 0.087
0.407 ± 0.073
6E10+, 82E1+ in 82E1+
0.6
0.4
0.2
0
wo/ HIER
w/ HIER

Figure4